Pergamon

Cement and Concrete Research 30 (2000) 1597–1607

CEMENT AND CONCRETE RESEARCH

Coupling between kinetics of dehydration, physical and mechanical behaviour for high alumina castable

Nicolas Schmitt[a,*], Jean-François Hernandez[a], Vincent Lamour[a,b], Yves Berthaud[a], Pierre Meunier[c], Jacques Poirier[d]

[a]*LMT-Cachan, ENS de Cachan, 61 avenue du Président Wilson, F-94 235 Cachan, France*
[b]*Department of Civil and Environmental Engineering, University of California, 451 Davis Hall, Berkeley, CA 94720-1710, USA*
[c]*LAFARGE Refractories, 97 avenue A. Briand, F-92 120 Montrouge, France*
[d]*SOLLAC, Grande Synthe, F-59 381 Dunkerque, France*

Received 3 January 2000; accepted 14 June 2000

Abstract

The dehydration of a high alumina cement castable and its influence on physical and thermomechanical behaviour is studied for temperatures below 800°C. The hydrated cement paste is composed of non-hydrated constituents (CA, CA_2 and $C_{12}A_7$) and two stable hydrates (AH_3 and C_3AH_6). The decomposition of the hydrates is analysed by TGA–DTA and XRD analyses. The complex chemical reactions are modelled by several kinetic laws characterising the conversion rate of the initial and intermediate formed hydrates. The variation of porosity and shrinkage of the cement paste as well as the shrinkage of the castable due to dehydration are also measured. A model, including local information at different micro-scales (constituents of the cement paste and their physical properties, volume fraction of aggregates), is proposed for both the paste and the castable.

Keywords: Kinetics; Shrinkage; Refractory cement; Thermal analysis; Physical properties

1. Introduction

The design of structures made of hydraulic-bonded ceramics and subjected to high thermal stresses is of great importance today. In high buildings or nuclear engineering, it is necessary to ensure a sufficiently long time the fire resistance of concrete structures even after they have cooled down and undergone again mechanical loads. The reliability of linings and pieces of refractories used in vessels (ovens, converters and ladles) must also be ensured because these structures are subjected to high temperatures under normal conditions. Past studies have been undertaken to model the thermomechanical behaviour of concrete and refractories.

For these materials the temperature range 20–800°C is of particular interest because, due to the dehydration, the cement undergoes significant microstructural transformations during the first thermal load. These transformations considerably modify the thermomechanical behaviour of the material and must be taken into account for a realistic structural analysis.

In the past, these phenomena were integrated into constitutive equations in different ways. In some studies, a classical thermomechanics formulation of homogeneous material has been used where the physical and mechanical properties depended only on temperature [1–3]. This approximation does not permit one to precisely describe the coupling between chemical-physics and mechanics in massive structures where great differences of transient regimes occur. Other approaches have been more realistic because they considered a multi-phase material (skeleton, liquid and vapour water) within the framework of mechanics of porous continua [4–8] to describe notably the transport of vapour and the pressure sometimes responsible for spalling and explosion. Based on this theory, only few thermomechanical models take into account the kinetics of the decomposition of hydrates by considering a global internal variable whose classical diffusion differential equation is identified by physical measurements [8,9].

In this paper, a description of the dehydration process and its consequence on the evolution of physical properties

* Corresponding author. Tel.: +33-1-4740-2836; fax: +33-1-4740-2240.
E-mail address: nicolas.schmitt@lmt.ens-cachan.fr (N. Schmitt).

0008-8846/00/$ – see front matter
PII: S0008-8846(00)00342-2

Table 1
Typical proportion in weight and volume of aggregates in alumina-castables

Castable (C)	CaO content (%)	Weight of cement (%)	Water to cement ratio	Density (kg m^{-3})	Volume of aggregates[a] (%)
Conventional C	>2.5	>10	0.5	2450	65
Low cement C	1–2.5	4–10	1	2900	65
Ultra low cement C	<1	<2	2.3	2900	65

[a] d>100 μm.

is based on experimental results. Relevant variables are proposed and constitutive equations describing their evolution are identified. Such an approach accounts for the real causes of transformation of the cementitious matrix. Once the transformations are characterised and the model parameters identified, it is possible to predict the kinetics of transformation for other initial compositions of ceramics (water–cement ratio or proportion of aggregates in the mixture) when using the same type of cement.

These results are used to characterise the shrinkage of ceramics due to dehydration. Homogenisation schemes are used to account for the local physical properties of the constituents of the refractory. Due to the complex microstructure of the cement paste, a simple approach is proposed to model its thermal strain during the decomposition of the hydrates. Then, a usual micromechanical model based on composite spheres is used to take into account the aggregates surrounded by the cement paste.

A heterogeneous ceramic with a high content of alumina is considered in the present work. This material is a refractory castable employed in steel manufacturing to achieve safe monolithic lining in ladles and other pieces that have to resist high temperatures. It follows that this material must resist temperatures up to the melting steel temperature (i.e., 1600°C).

2. Dehydration of alumina refractories

2.1. Composition of material before dehydration

The refractory was made of particles embedded in a hydraulic binder phase. The aggregates are composed of bauxite for the coarser sizes up to 3.5 mm and fine white fused alumina (1–10 μm). The particle size distribution followed the Andreassen's distribution to reduce porosity. The proportion of aggregates in such refractories may be variable depending on the type of refractory required for the application (Table 1).

Table 2
Chemical composition of cement before hydration

Constituent	CA	CA_2	$C_{12}A_7$
Weight (%)	61	37.5	1.5

The cement used in this study was a SECAR 71 made by Lafarge Aluminate. Its composition is given in Table 2 [10]. It is composed mainly of CA, CA_2 and $C_{12}A_7$ aluminate compounds where the Bogue's notation is used.[1]

The cementitious matrix was obtained by a partial hydration of the calcium aluminate cement (water–cement ratio w/c = 0.3). After hydration, several types of hydrates were obtained (CAH_{10}, C_2AH_8, C_3AH_6 and AH_3) depending on the setting and hardening temperature. But it is well known that the hexagonal hydrates CAH_{10} and C_2AH_8 are metastable and convert slowly into the stable hydrates C_3AH_6 and AH_3. In the refractory industry the classical reference state for these materials is obtained by curing the specimen at 120°C to eliminate the non-chemically bonded water and to accelerate the conversion process. The specimens tested were previously heated at 120°C for 48 h so that only two stabilised hydrates, AH_3 and C_3AH_6, were formed by the global reactions (Eqs. (1a)–(1c))

$$3CA + 12H \rightarrow C_3AH_6 + 2AH_3 \quad (1a)$$

$$3CA_2 + 21H \rightarrow C_3AH_6 + 5AH_3 \quad (1b)$$

$$C_{12}A_7 + 33H \rightarrow 4C_3AH_6 + 3AH_3 \quad (1c)$$

The main constituents of the cementitious matrix were observed by X-ray diffraction analysis (Fig. 1). Their amounts (see Table 3, line a) were estimated for the ratio w/c = 0.3 by assuming that the kinetics of CA and CA_2 reactions are the same and that 5% (in weight) of the initial water content was chemically free (as confirmed by experiment). The volume content of hydrated cement was calculated using both the densities of compounds proposed in the literature [10] and the measured porosity of 14%. It can be seen that only 70% in weight of the matrix is hydrated. These proportions are very sensitive to the w/c ratio.

2.2. Evolution of the cementitious matrix during dehydration

X-ray diffraction analyses made on specimens heated at different temperatures (up to 600°C) show that the hydrated phases are decomposed into several complex

[1] C = CAO, A = Al_2O_3, S = SiO_2 and H = H_2O.

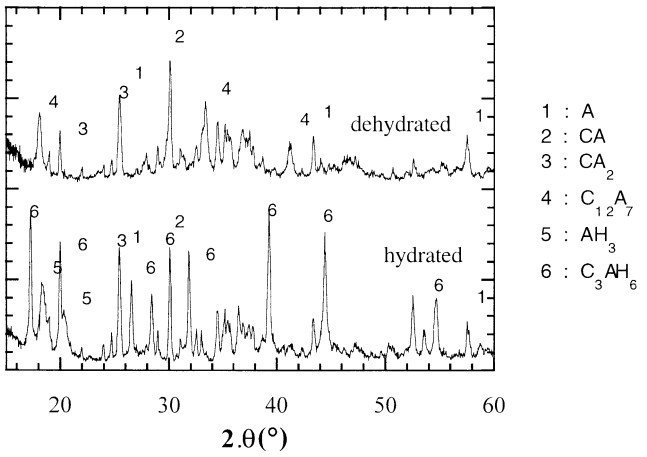

Fig. 1. X-ray diffractograms of a cementitious paste treated at 120°C (hydrated) and 600°C (dehydrated).

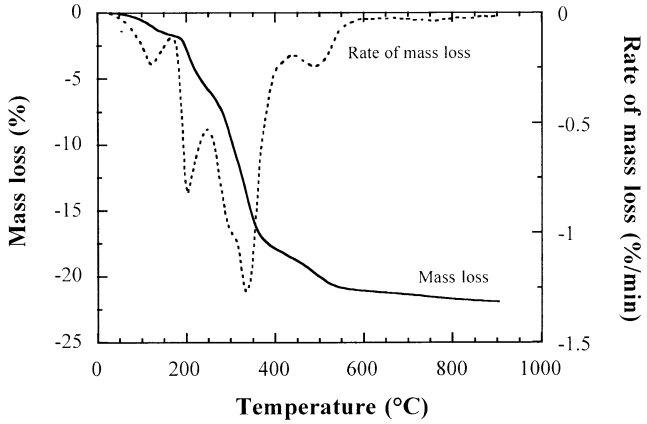

Fig. 2. TGA mass loss of cementitious matrix (w/c = 0.3).

phases. As a first approximation, the chemical reactions may be described by the following equations [10,11]

$$AH_3 \rightarrow AH + 2H \quad (2a)$$

$$AH \rightarrow A + H \quad (2b)$$

$$C_3AH_6 \rightarrow C_3AH_{1.5} + 4.5H \quad (3a)$$

$$C_3AH_{1.5} \rightarrow (C_{12}A_7, CA, CA_2, CA_7, A) + 1.5H \quad (3b)$$

As shown by Kuzel [12] and Richard [13], first C_3AH_3 decomposes into two phases $C_{12}A_7H$ and CH whose chemical condensed writing is $C_3AH_{1.5}$ (Eq. (3a)). The CH phase is scattered in the structure of $C_{12}A_7H$. Then the decompositions of $C_{12}A_7H$ and CH occur and produce $C_{12}A_7$ and C. These phases react with A and give CA and CA_2. A condensed notation X=($C_{12}A_7$, CA, CA_3, A,...) is used to describe these reactions.

During the decomposition, the chemically bonded water becomes free and changes into vapour that is eliminated. As a consequence a mass loss of the specimen can be observed. A classical way to study the kinetics of this phenomenon consists in making thermogravimetric analysis (TGA) and differential thermal analysis (DTA). Exploratory differential thermal analyses were carried out on 1 to 2 g samples with a low constant heating rate of 10°C min^{-1}. A typical result obtained by TGA on the cementitious matrix is shown in Fig. 2.

The different stages of the previously described dehydration process have been observed. The first peak of mass loss rate is due to the elimination of the zeoletic water. The other peaks resulted in the decomposition of hydrates. The hydrate AH_3 lost at first two molecules of water and later on the third one. The hydrate C_3AH_6 freed the principal molecules of water and later at higher temperature the remaining molecules. This analysis was confirmed by the thermogram of DTA that exhibited the same temperature peak.

Fig. 3 shows the influence of the temperature loading history. The different points reported correspond to tests where the temperature was first increased to an upper value and then maintained at this level for 3 h. Therefore, one may consider that the dashed line curve roughly corresponds to a TGA test with a very low temperature increasing rate.

2.3. Effects of dehydration on porosity and shrinkage

During the decomposition process, the structures of the initial phases become denser. For example, the density of AH_3 is nearly 2420 kg m^{-3}. After dehydration, it is

Table 3
Chemical composition of cement in weight and volume before hydration (a) and after curing at 120°C (b) for water to cement ratio w/c = 0.3

Constituent	CA	CA_2	$C_{12}A_7$	H_2O	AH_3	C_3AH_6
Weight a (%)	46.92	28.85	1.15	23.08	0	0
Weight b (%)	15.74	14.20	0.0	0	36.31	33.75
Volume b (%)	11.77	10.87	0	0	33.44	29.85

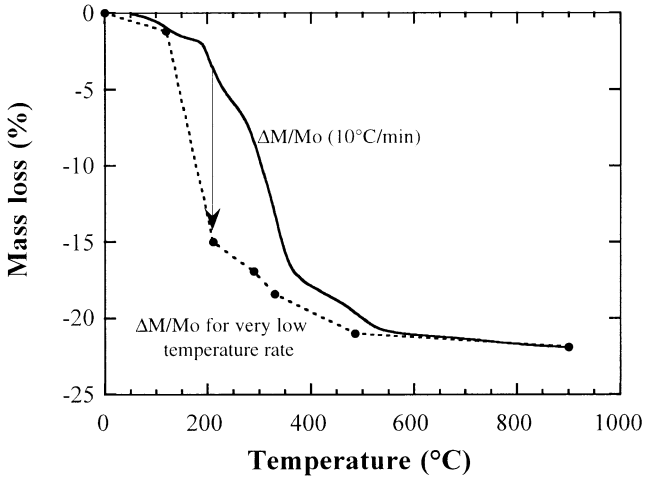

Fig. 3. Influence of the temperature rate on the mass loss of cementitious matrix (w/c = 0.3).

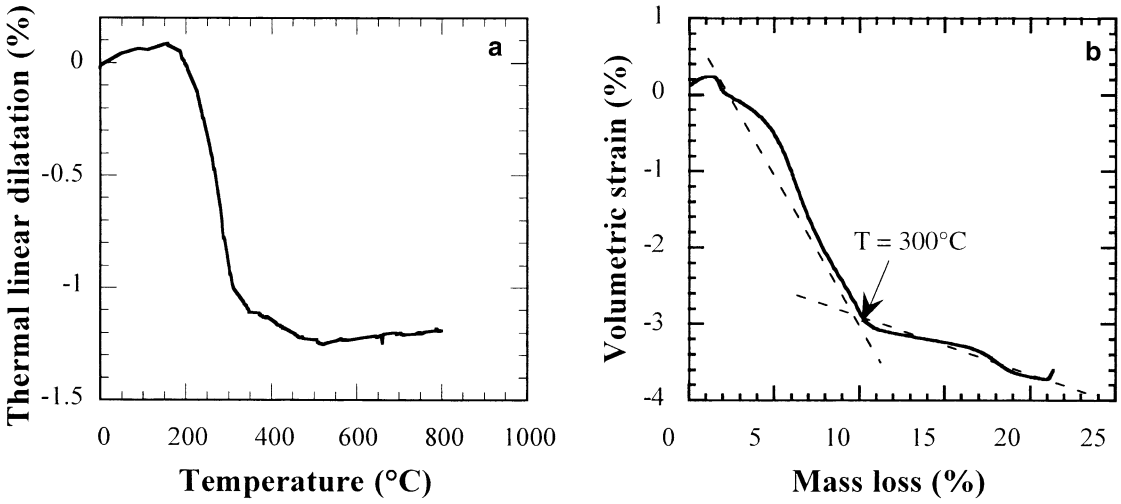

Fig. 4. Change of the thermal strain with temperature or mass loss of the cementitious paste (w/c = 0.3).

transformed into alumina whose density is equal to 3970 kg m^{-3} when considered as a perfect crystal. The corresponding volume reduction is about 60%. The volume reduction of C_3AH_6 is about 43%. In fact, the apparent density of the phases is less than the theoretical density because the structure is more or less amorphous. Moreover, the hydrates are scattered in the porous matrix containing also non-hydrated phases. They are surrounded by anhydrous phases that constrain the shrinkage of the decomposed phases.

Fig. 4a shows the change of the thermal strain observed during the first heating of the cement paste for a monotonic temperature rate of 10°C min^{-1}. These tests were carried out by using an in-house device on hollow cylinders with an inner diameter of 8 mm, an outer diameter of 25 mm and 40 mm in length. A differential displacement measurement device between the top and the bottom of the specimen was used to measure the thermal dilatation. The shrinkage observed is an irreversible phenomenon that remains after cooling down the material. For this composition, the uniaxial shrinkage is about 1.4%. In Fig. 4b, the volumetric shrinkage is related to the mass loss. One can note that two regimes occur with different slopes. In the first regime the shrinkage is fast (with a slope equal to 0.31). The mass loss mainly corresponds to the reactions of Eqs. (2a) and (3a) and is accompanied by a densification of the material. In the second regime the shrinkage is noticeably lower (slope equal to 0.072). One can suppose that the progressive loss of matter does not affect the volume of the crystals when the hydrated phases transform into dehydrated phases. In particular the decomposition of

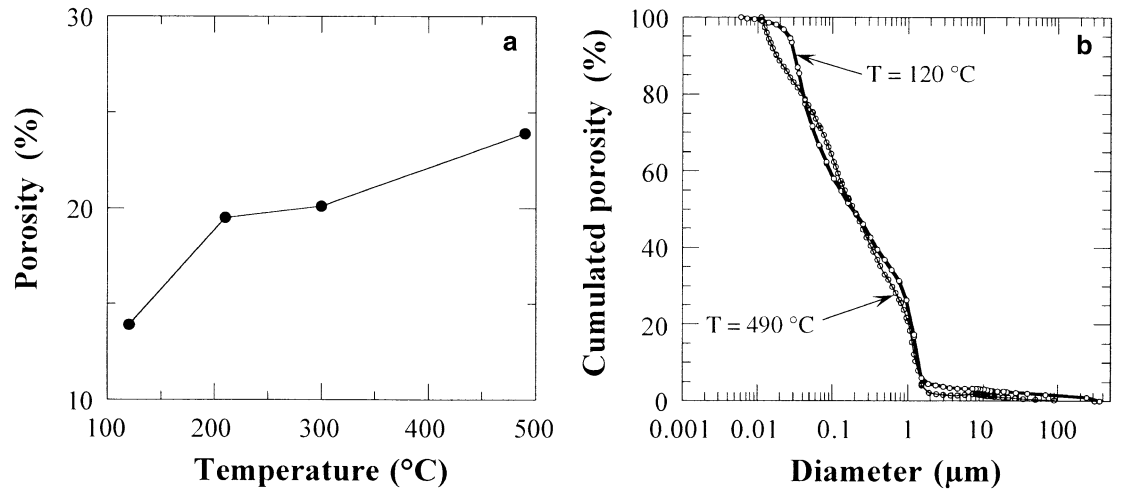

Fig. 5. Change of porosity with temperature of void diameter of the cement paste (w/c = 0.3).

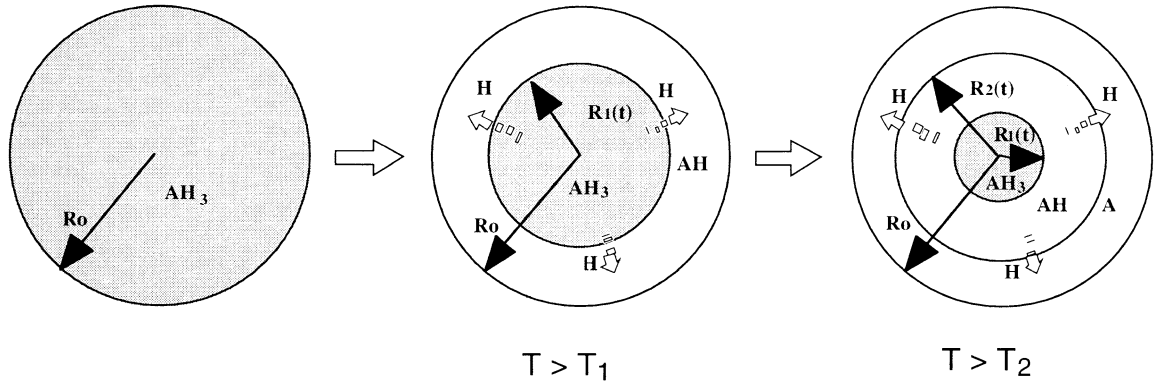

Fig. 6. Topology of the dehydration process of AH_3.

$C_{12}A_7H$ in $C_{12}A_7$ does not change the density of the phase [13].

The connected porosity of the cement paste was measured after the heat treatments of the specimens by Mercury Intrusion Porosimetry test (M.I.P.). Micro voids and flaws are present in the material in high proportion (14%). During the chemical transformations, the porosity increases from 14% to 24% (Fig. 5a). But this increase does not modify the distribution of void sizes in the paste (Fig. 5b).

3. Modelling of the dehydration process of the cementitious matrix

To model the kinetics of a chemical reaction, the usual way consists in introducing a variable ζ defining the degree of advancement of reaction whose rate is defined by

$$\frac{d\zeta}{dt} = k(T)(1 - \zeta)^n \tag{4}$$

where $k(T)$ is a rate constant following the Arrhenius' law and n represents the order of the reaction. In this study, the dehydration process may be roughly viewed as indicated in Fig. 6 for the case of the hydrate AH_3. All hydrates AH_3 are grouped together in spheres whose initial radius is denoted by R_{oi}. Upon heating, the first spherical shell of reacted phase AH occurs as soon as the temperature exceeds T_1 and radially enlarges towards the centre of the composite sphere. The reaction Eq. (2a) produces along the interface (inner radius R_1) and the vapour is diffused through the shell. When the temperature exceeds a second limit T_2, AH transforms into A and a second spherical shell (inner radius $R_2 \geq R_1$) appears and progresses radially. The variables ζ_i can thus be defined by

$$\zeta_i = 1 - \frac{r_i^3(t)}{R_{oi}^3(t)}. \tag{5}$$

It is assumed that the water vapour released during the reaction diffuses through the shell without flow resistance. By introducing Eq. (5) and its time derivative in Eq. (4), it can be shown that the order of reaction n is equal to 2/3 if the front of reaction moves with a constant rate for a given temperature. This assumption is too restrictive in the case of hydration because the diffusion of water through the hydrate formed is low. Finally, the kinetics of dehydration reactions can be written as in Eqs. (6) and (7).

Reactions corresponding to Eqs. (2a) and (3a)

$$\begin{aligned} &T < T_i \quad \frac{d\zeta_i}{dt} = 0 \quad \text{and} \quad T \geq T_i \\ &\frac{d\zeta_i}{dt} = -K_i(1 - \zeta_i)^{2/3}\exp\left(-\frac{E_i}{RT}\right) \end{aligned} \tag{6}$$

for $i=\{1,3\}$ and $0 \leq \zeta_i \leq 1$.

Reactions corresponding to Eqs. (2b) and (3b)

$$\begin{aligned} &T < T_i \; \frac{d\zeta_i}{dt} = 0 \quad i = \{2,4\} \quad 0 \leq \zeta_i \leq 1 \\ &T > T_i \text{ and } \zeta_i \leq \zeta_{i-1} \\ &\frac{d\zeta_i}{dt} = K_i(1 - \zeta_i)^{2/3}\exp\left(-\frac{E_i}{RT}\right) \\ &T > T_i \text{ and } \quad \zeta_i = \zeta_{i-1} \quad \frac{d\zeta_i}{dt} = \frac{d\zeta_{i-1}}{dt} \end{aligned} \tag{7}$$

In these expressions T_i, K_i and E_i are, respectively, the temperature threshold, the reaction rate and the apparent

Table 4
Kinetic parameters of dehydration of hydrates

Reaction	T_i (°C)	K_i (min^{-1})	E_i (kJ mol^{-1})	n_i
2a	110	8.0	18000	2/3
3a	175	0.415	21000	2/3
2b	310	2.5	11000	2/3
3b	235	1.55	19000	2/3

activation energy for reaction (i), with R as the universal gas constant and T the absolute temperature.

The intrinsic parameters T_i, K_i and E_i are identified by TGA and TDA analyses with specimens heated with differ-

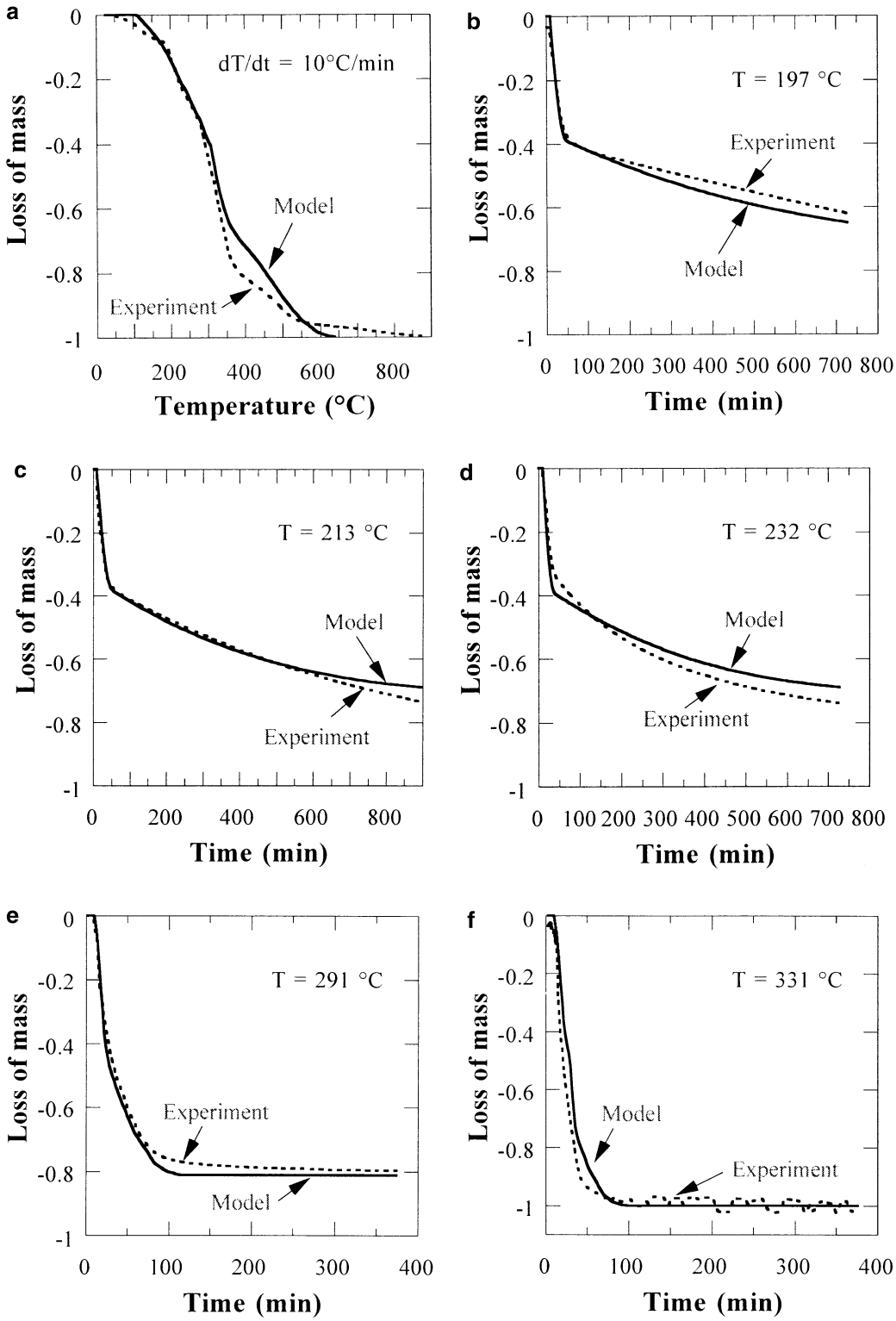

Fig. 7. Mass loss in a cementitious matrix (w/c = 0.3): comparison between model and experimental data.

ent time–temperature histories. The unit mass loss ml(t) is given by the following expression [Eq. (8)]

$$\mathrm{ml}(t) = \frac{\mathrm{Mp}(0) - \mathrm{Mp}(t)}{\mathrm{Mp}(0)} = \frac{\mathrm{Mp^A}(0) - \mathrm{Mp^A}(t) + \mathrm{Mp^C}(0) - \mathrm{Mp^C}(t)}{\mathrm{Mp}(0)} \quad (8)$$

with

$$\mathrm{Mp^A}(t) = [(1 - \zeta_1) + \zeta_1(1 - \zeta_2) f_{\mathrm{cm}}(\mathrm{AH}) + \zeta_1\zeta_2 f_{\mathrm{cm}}(\mathrm{A})] f_{\mathrm{m}}(\mathrm{AH_3})\mathrm{Mp}(0), \quad (9a)$$

$$\mathrm{Mp^C}(t) = [(1 - \zeta_3) + \zeta_3(1 - \zeta_4) f_{\mathrm{cm}}(\mathrm{C_3AH_{1.5}}) + \zeta_3\zeta_4 f_{\mathrm{cm}}(\mathrm{X})] f_{\mathrm{m}}(\mathrm{C_3AH_6})\mathrm{Mp}(0). \quad (9b)$$

In Eqs. (9a) and (9b), Mp(0) is the initial mass of the cement paste, $f_{\mathrm{m}}(\mathrm{AH_3})$ and $f_{\mathrm{m}}(\mathrm{C_3AH_6})$ are the mass proportion of the hydrates contained in Mp(0). The proportions f_{m} depend on the initial composition of the cement and the w/c ratio. The quantities $f_{\mathrm{cm}}(\mathrm{AH})$ and $f_{\mathrm{cm}}(\mathrm{A})$ are the mass proportions of constituents remaining after transformation of the mass $M(\mathrm{AH_3})$. Similarly, $f_{\mathrm{cm}}(\mathrm{C_3AH_{1.5}})$ and $f_{\mathrm{cm}}(\mathrm{X})$ are the mass proportions remaining after transformation of the mass $\mathrm{M(C_3AH_6)}$. They are calculated using the stoechiometric equations [Eqs. (2a)–(3b)].

The following approach was used to identify the parameters. The temperature thresholds have been identified from the derivative thermogravimetric analysis curves that presented several peaks corresponding to different chemical reactions. Then the parameters governing the successive reactions have been identified by using the two-step loading curves and the classical one-step loading curve.

The identified parameters of the kinetic laws are reported in Table 4. This procedure leads to a set of material parameters (probably not unique) that seems reasonable. Fig. 7 shows a good agreement between experimental data and the model predictions. In these figures, the mass loss is normalised by the maximum mass loss reached after total dehydration. It is worth noting that this identification must be performed once. The change of water–cement ratio only modifies the initial degree of hydration and not the material parameters.

4. Identification of the thermal dilatation and the porosity of the cementitious paste

The thermal strain $\varepsilon_{\mathrm{vp}}^{\mathrm{th}}$ of the cementitious paste (see Fig. 4a) is due to both the usual thermal strain $\varepsilon_{\mathrm{vp}}^{\alpha}$ induced by a temperature change and the shrinkage strain $\varepsilon_{\mathrm{vp}}^{\mathrm{sh}}$ which is specific to the decomposition of the hydrates (Fig. 4b). The total thermal strain is divided into two parts [Eq. (10)]

$$\varepsilon_{\mathrm{vp}}^{\mathrm{th}} = \varepsilon_{\mathrm{vp}}^{\alpha} + \varepsilon_{\mathrm{vp}}^{\mathrm{sh}}. \quad (10)$$

The thermal strains can be identified on the basis of the experimental data considering the macroscopic point of view. In the present work, it seems to us interesting to take into account information on the different compounds of the cement paste. But it is not easy to choose an homogenisation scheme because the microstructure of the paste is complex and changes notably during the decomposition of hydrates. For these reasons an alternative way is chosen to elaborate a model that allows us to show the influence of local material parameters on the thermal strains.

The thermal strain $\varepsilon_{\mathrm{vp}}^{\alpha}$ depends on the temperature variation in a reversible way for a given chemical state of the material [Eq. (11)]

$$\varepsilon_{\mathrm{vp}}^{\alpha} = 3\alpha(T, \zeta_i)(T(t) - T_0) \quad (11)$$

where $\alpha(T,\zeta_i)$ is the coefficient of linear thermal expansion. This material parameter varies with the temperature but also the composition of the cement paste. T_0 is the reference temperature. A linear dependence of $\alpha(T,\zeta_i)$ with the mass loss is a reasonable approximation because during the decomposition the variation of $\varepsilon_{\mathrm{vp}}^{\alpha}$ is much smaller than the shrinkage strain (Eq. (12))

$$\alpha(T, \zeta_i) = \left(1 - \frac{\mathrm{ml}(\zeta_i(t))}{\mathrm{ml}(\zeta_i = 1)}\right)\alpha(\text{hydrated state}, T) + \frac{\mathrm{ml}(\zeta_i(t))}{\mathrm{ml}(\zeta_i = 1)}\alpha(\text{dehydrated state}, T). \quad (12)$$

The following expressions have been identified for the coefficients of thermal expansion.

$\alpha(\text{hydrated state}, T) = 1.6 \times 10^{-5} + 1.6 \times 10^{-8} T$
$20°\mathrm{C} < T < 150°\mathrm{C}$

$\alpha(\text{dehydrated state}, T) = 0.65 \times 10^{-5} + 1.8 \times 10^{-8} T$
$200°\mathrm{C} < T < 700°\mathrm{C}.$

The second part corresponds to an irreversible volumetric contraction due to dehydration. To understand the effects of the major factors let us consider at first the ideal case where only hydrates are initially present in the cement paste. If each crystal (initial hydrate or intermediate hydrate) shrinks without interaction with the other crystals and if no porosity is present in the cement paste, the overall volume variation of the cementitious matrix is obtained by addition of the volume variation of each phase. Then the volumetric shrinkage strain of the cement paste $\varepsilon_{\mathrm{v}}^{\mathrm{sh}}(t)$ writes [Eq. (13)]

$$\varepsilon_{\mathrm{v}}^{\mathrm{sh}}(t) = \varepsilon_{\mathrm{v}}^{\mathrm{cs}}(t) \quad (13)$$

with

$$\varepsilon_{\mathrm{v}}^{\mathrm{cs}}(t) = \varepsilon_{\mathrm{v}}^{\mathrm{csA}}(t) + \varepsilon_{\mathrm{v}}^{\mathrm{csC}}(t)$$

$$\varepsilon_{\mathrm{v}}^{\mathrm{csA}}(t) = \frac{V^{\mathrm{A}}(t) - V^{\mathrm{A}}(0)}{V^{\mathrm{A}}(0) + V^{\mathrm{C}}(0)} \quad \text{and}$$

$$\varepsilon_{\mathrm{v}}^{\mathrm{csC}}(t) = \frac{V^{\mathrm{C}}(t) - V^{\mathrm{C}}(0)}{V^{\mathrm{A}}(0) + V^{\mathrm{C}}(0)}$$

$$V^{A}(t)= \left[\frac{1}{\rho(AH_3)}(1-\zeta_1)+\zeta_1(1-\zeta_2)\frac{f_{cm}(AH)}{\rho(AH)} +\zeta_1\zeta_2\frac{f_{cm}(A)}{\rho(A)}\right]f_m(AH_3)Mc(t_0)$$

$$V^{C}(t) = \left[\frac{1}{\rho(C_3AH_6)}(1-\zeta_3) + \zeta_3(1-\zeta_4)\frac{f_{cm}(C_3AH_{1.5})}{\rho(C_3AH_{1.5})} + \zeta_3\zeta_4\frac{f_{cm}(X)}{\rho(X)}\right]f_m(C_3AH_6)Mc(t_0)$$

where $V^{A}(t)$, $V^{C}(t)$ are the volumes of AH_3, C_3AH_6, respectively, and $\rho(s)$ is the density of the constituent (s).

In reality there exist many interactions at different scales of the cementitious paste due to heterogeneity. Both hydrate grains and non-hydrated grains are present at the initial stage and at the hydrate grain scale, intermediate layers occur during dehydration. The incompatibility of thermomechanical strains leads to a reduction of the apparent shrinkage of the cement paste that could be taken into account by the following expression (Eq. (14))

$$\varepsilon_{vp}^{sh}(t) = H(AH_3)\varepsilon_v^{csA}(t)f_v(AH_3) + H(C_3AH_6)\varepsilon_v^{csC}(t)f_v(C_3AH_6) \quad (14)$$

where $f_v(AH_3)$ and $f_v(C_3AH_6)$ are the volume fractions of the hydrates contained in the cement paste before dehydration, $H(AH_3)$ and $H(C_3AH_6)$ are interaction parameters. These parameters can be evaluated by using a micromechanical approach with a multi-scale homogenisation scheme such as the one developed by Burr [14]. However, such an approach does not take into account the increase of the porosity due to either voids appearing around a grain that shrinks without interaction with the surrounding grains or voids induced by a damage mechanism. The effect of the porosity on the shrinkage is introduced by considering that the total volume variation of the paste is the sum of the volume changes of the solid skeleton and the voids. It results

$$\varepsilon_{vp}^{sh}(t) = \frac{1-\phi_0}{1-\phi(t)}[H(AH_3)\varepsilon_v^{csA}(t)f_v(AH_3) + H(C_3AH_6)\varepsilon_v^{csC}(t)f_v(C_3AH_6)] + \frac{\phi(t)-\phi_0}{1-\phi(t)}. \quad (15)$$

For the sake of simplicity, the interaction parameters $H(AH_3)$ and $H(C_3AH_6)$ are supposed to have the same value and are identified on a set of experimental data. One can note that a volume variation can be observed in Eq. (15) even with no chemical shrinkage. The experimental results actually suggest that the porosity variation $\phi(t)$ is a function of the

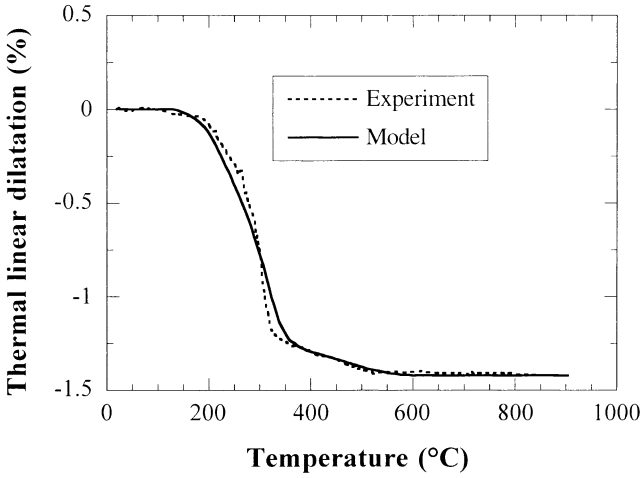

Fig. 9. Measured and predicted linear shrinkage versus temperature (heat rate 10°C min^{-1}).

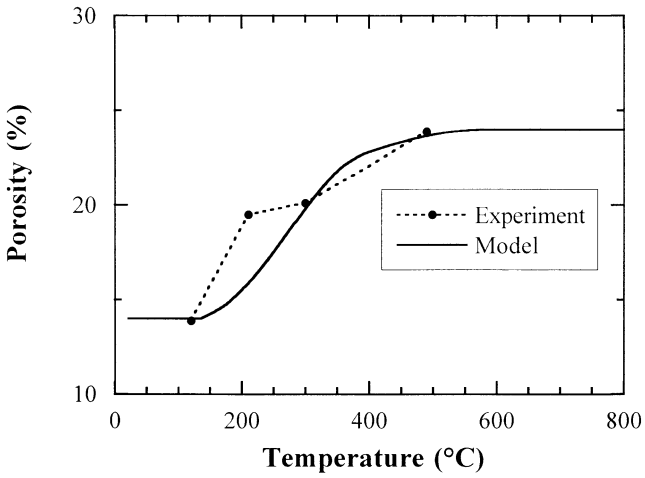

Fig. 8. Comparison between predicted and measured porosities vs. temperature.

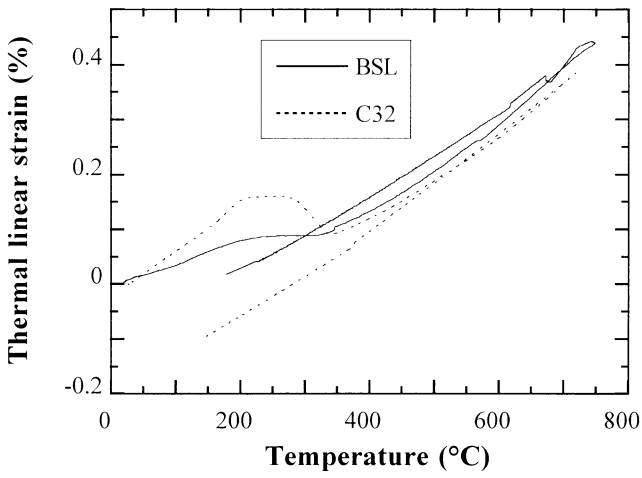

Fig. 10. Thermal linear expansion for a conventional castable (C32) and an ultra low cement castable (BSL) (identical cement and w/c = 0.3).

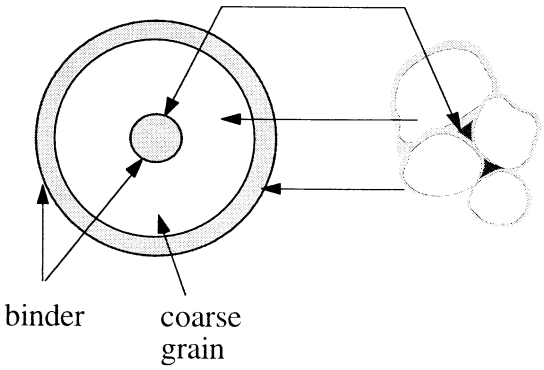

Fig. 11. Topology of the De Larrard and Le Roy model.

chemical shrinkage of the hydrates. As a first approximation a linear variation of the porosity from an initial value ϕ_0 to a final value $\phi_0 + \Delta\phi$ is assumed [Eq. (16)]

$$\phi(t) = \phi_0 + \delta\phi \frac{\varepsilon_v^{cs}(t)}{\varepsilon_v^{cs}(\infty)}. \quad (16)$$

In practice, ϕ_0 and $\Delta\phi$ are given by M.I.P. (ϕ_0 = 14% and $\Delta\phi$ = 10%). This approximation leads to an underestimation of ϕ_0 because the interlayer space in the hydrated phases and the closed porosity are not included. Moreover, in reality $\Delta\phi$ is probably less than 10% because a part of initial closed porosity changed to connected porosity during the heat treatment. Fig. 8 shows the results of this approximation.

Fig. 9 gives the evolution of the uniaxial shrinkage $\varepsilon_p^{sh}(t)=(1/3)\varepsilon_{vp}^{sh}(t)$ during the first thermal loading obtained both by experiment and the model. It can be noted that the shrinkage of the cement paste depends on three composition parameters, the porosity, and the strain restrained parameters $H(i)$. It is then possible with such a model to predict the shrinkage of the cement paste according to the ratio (w/c) or the influence of the initial chemical composition of the cement.

5. Shrinkage of refractory

Shrinkage occurring in concrete has been widely studied in the past. Fig. 10 shows the thermal strains for a high cement content castable and an ultra low cement castable during heating followed by cooling. It highlights the differences of shrinkage that are due to both the composition of the cement paste and the volume content of aggregates.

The shrinkage of concrete can be related to the shrinkage of the cement paste and the concentration of the aggregates by using micromechanical approaches. Christensen and Lo [15,16] have developed semi-analytical solutions to determine the thermo-elastic properties of two phase composites composed of spherical-shaped inclusions embedded in a continuous matrix. Later the Generalised Self-Consistent Scheme has been extended for multi-phase inclusions by Siboni and Benveniste [17]. Another approach has been developed by Hashin [18] and Hashin and Rosen [19] giving explicit analytical solutions. It is based on a particular packing of composite spheres completely filling the material. An extension of the composite spheres packing has been proposed recently by de Larrard and Le Roy [20,21]. In this model (Fig. 11) the coarse grains are coated with only a part of the matrix phase. The other part is trapped in the void between the composite spheres, because the densest aggregate packing does not permit to fill up the void space.

The expression of the volumetric shrinkage of the refractory $\varepsilon_{vr}^{sh}(t)$ is obtained by considering that the Poisson's coefficient of the matrix, the inclusions and the composite is equal to 0.2. This approximation is satisfactory for common concrete as shown by de Larrard and Le Roy [21] so that $\varepsilon_{vr}^{sh}(t)$ can be expressed as [Eq. (17)]

$$\varepsilon_{vr}^{sh}(t) = \left[\frac{(1+E)(1-b) + \frac{4E(1-a^*)b}{a^*+E(2-a^*)}}{1+b+E(1-b)}\right]\varepsilon_{vp}^{sh}(t) \quad (17)$$

with $E=(E_p/E_a)$, $b=(a/a^*)$ and E_p E_a Young's modulus of cementitious matrix and aggregates, respectively, with a as

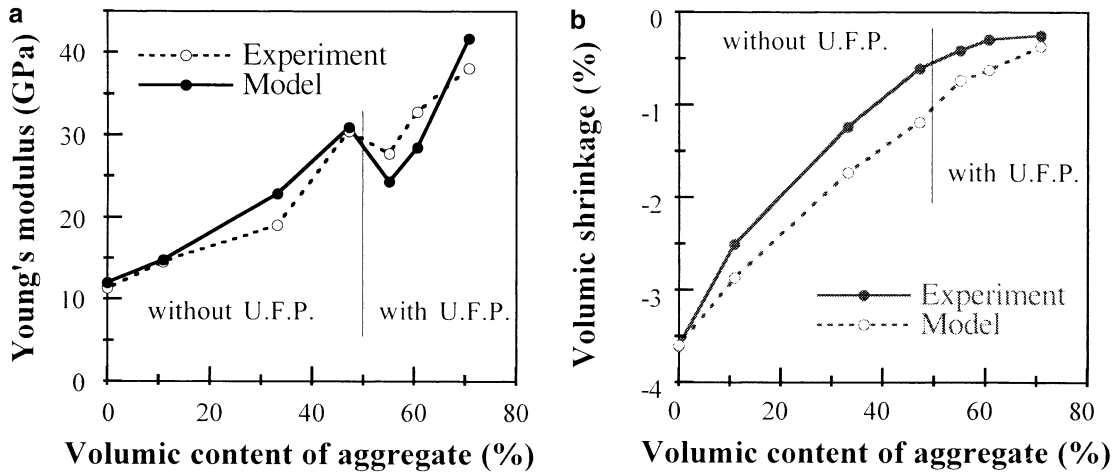

Fig. 12. Comparison between experiments and model prediction of a heat-treated specimen of castable.

the volumetric fraction of aggregates, a^* the volumetric fraction for the maximum compaction and $\varepsilon_{vp}^{sh}(t)$ the volumetric shrinkage of the cement paste.

Rosen and Hashin's model can easily be obtained considering the maximal aggregate content a^* equal to 1. In Eq. (17) the parameters a^* and E must be adjusted. A value of 0.88 is used for a^*. This value is a medium value for high strength concrete. The ratio of Young's moduli has been determined by ultrasonic measurement of specimens (after heat treatment) with different aggregates content by using the ''three sphere'' model ($E = 0.1$). The Young's modulus of the castable writes [Eq. (18)]

$$E_r = \left[1 + \frac{2b(1 - E^2)}{(1 - b) - 2(1/2/a^*)E + (1 + b)E^2}\right]E_c. \quad (18)$$

Fig. 12a and b shows that the model is able to predict the experimental data with reasonable accuracy. The slope change in Fig. 12 is due to the addition of ultra fine powders (U.F.P.) of alumina and silica fume for high content of aggregates. For this case, the micromechanical model has been applied twice. In a first step, the Young's modulus and the shrinkage strain of a phase containing the cement paste and only the very small particles are calculated. In the second step, this phase is considered as the matrix of the castable containing coarse aggregates, so that the model can be applied again.

6. Conclusion

The physico-chemical behaviour of high cement ceramic has been examined. On the basis of TGA and DTA results, a fine modelling of the kinetics of dehydration of the cement paste has been developed and identified. This description takes into account local information on the composition of the cement and the water to cement ratio to calculate the proportion of formed hydrates. The parameters are identified so that they can be used to predict the mass loss of hydrate cement paste for different water to cement ratios or for cement with other proportions of anhydrous phases.

Physical transformations of cement paste and castable have been studied. In particular, the macroscopic evolution of shrinkage is modelled by using a multi-scale analysis. Again, local information is taken into account for the identification. The influences of the volume fraction of each hydrate and of the concentration of aggregates are explained.

The results and the proposed model can be of great interest for a more accurate description of the coupling between chemical and physico-mechanical phenomena. It is an alternative route to improving the classical phenomenological approaches.

Acknowledgments

The research was supported by SOLLAC France and LAFARGE Refractories companies.

References

[1] A. Khennane, G. Baker, Thermoplasticity model for concrete under transient temperature and biaxial stress, Proc R Soc London, Ser A 439 (1992) 59–80.
[2] K.-C. Thienel, F.S. Rostasy, Strength of concrete subjected to high temperature and biaxial stress: experiments and modelling, Mater Struct 28 (1995) 575–581.
[3] G. Heinfling, J.M. Reynouard, C. Duval, Modelling of concrete behaviour at elevated temperatures within the framework of thermo-plasticity, in: R.I.o. Technology (Ed.), Thermal Stresses '97 Second Int. Symp. on Thermal Stresses and Related Topics, Rochester, NY, USA, Pub., 1, 1997, 77–80.
[4] Z.P. Bazant, W. Thonguthai, Pore pressure and drying of concrete at high temperatures, ASCE J Eng Mech 104 (EM5) (1978) 1059–1079.
[5] Z.P. Bazant, Mathematical model for creep and thermal shrinkage of concrete at high temperature, Nucl Eng Des 76 (1983) 183.
[6] C.E. Majorana, B.A. Schrefler, High temperature behaviour of concrete as an unsaturated porous material, in: S. University (Ed.), Thermal Stresses '95, Hamamatsy Japon, Pub., 1995, 417–420.
[7] Z.X. Gong, A.S. Mujumdar, Development of drying schedules for one-side-heating drying of refractory concrete slabs based on a finite element model, J Am Ceram Soc 79 (6) (1996) 1649–1658.
[8] M. Jouhari, I. Laalai, A constitutive model for thermo-hydro-chemo-mechanical response of decomposing high performance concrete under high temperature, in: R.I.o. Technology (Ed.), Thermal Stresses '97 2th Int. Symp. on Thermal Stresses and Related Topics June 8–11, 1997, Rochester, NJ, USA, Pub., 1997, 221–225.
[9] F.J. Ulm, O. Coussy, Z.P. Bazant, The chunnel fire: I. Chemoplastic softening in rapidly heated concrete, J Eng Mech 9 (March) (1999) 272–282.
[10] S. Plibrico, Technology of Monolithic Refractories, Plibrico Japan, Tokyo, Japan, 1984.
[11] G. Platret, Processus de formation et propriétés des produits de déshydratation de CAH10, PhD Thesis, University of Dijon, 1983 (in French).
[12] H.J. Kuzel, Uber die orientierte Entwässerung von Tricalciumaluminathydrate C_3AH_6, Neues Jahrb Mineral Monatheft 9 (in German) (1969) 397–403.
[13] N. Richard, Structure et propriétés élastiques des phases cimentières à base de mono-aluminate de calcium, PhD Thesis, University of Paris 6, France, 1995 (in French).
[14] A. Burr, Micromécanique et comportement de matériaux hétérogènes, PhD Thesis, University of Paris, Paris France, 1995 (in French).
[15] R.M. Christensen, K.H. Lo, Solutions for effective shear properties in three phase sphere and cylinder models, J Mech Phys Solids 27 (1979) 315–330.
[16] R.M. Christensen, K.H. Lo, Solutions for effective shear properties in three phase sphere and cylinder models (erratum), J Mech Phys Solids 34 (1986) 639.
[17] G. Siboni, Y. Beneveniste, A micromechanics model for the effective thermomechanical behavior of multiphase composite media, Mech Mater 2 (11) (1991) 107–122.
[18] Z. Hashin, The elastic moduli of heterogeneous materials, J Mech Phys Solids 29 (1962) 143.

[19] B.W. Rosen, Z. Hashin, On the coefficients of thermal expansion of heterogeneous materials, Int J Eng Sci 8 (1970) 157.
[20] F. de Larrard, R. Le Roy, Un modèle géométrique d'homogénéisation pour les composites bi-phasiques à inclusion granulaire de large étendue, C R Acad Sci Paris (in French) 314 (II) (1992) 1253–1257.
[21] F. de Larrard, R. Le Roy, The influence of mix composition on mechanical properties of high-performance silica fume concrete, in Istanbul, Turkey, Pub. (Ed.), 4th Int. Conf. on Fly Ash, Silica Fume, Slag and Natural Pozzolans in Concrete, 1992.